

Extended Tidal Tails of IC 4756 detected by *Gaia* EDR3

XIANHAO YE,^{1,2} JINKUN ZHAO,¹ JIAJUN ZHANG,^{1,2} YONG YANG,^{1,2} AND GANG ZHAO^{1,2}

¹*CAS Key Laboratory of Optical Astronomy, National Astronomical Observatories, Chinese Academy of Sciences, Beijing 100101, China*

²*School of Astronomy and Space Science, University of Chinese Academy of Sciences, Beijing 100049, China*

(Received 2021 May 24; Revised 2021 August 13; Accepted 2021 August 17; Published 2021 September 30)

Submitted to AJ

ABSTRACT

We report the discovery of emerged tidal tails around open cluster IC 4756 (~ 1 Gyr) based on 644 members identified from *Gaia* EDR3. Three-dimensional spatial positions, two-dimensional tangential velocities ($x, y, z, \kappa \cdot \mu_{\alpha}^*/\varpi, \kappa \cdot \mu_{\delta}/\varpi$) are utilized to determine the co-moving member candidates of IC 4756. Using a Bayesian method, we correct the distance for each cluster member. Two tidal tails extend up to 180 pc and display a S-shape in $X'Y'$ space (Cartesian coordinates focused on cluster center). A clean sequence of our members in Color-Absolute-Magnitude Diagram (CAMD) indicates the coeval population and matches perfectly with the PARSEC isochrone with age from Bossini et al. (2019). Mass segregation is detected in this cluster as well. Finally, we derive the tidal radius and core radius of IC 4756 about 12.13 pc and 4.33 ± 0.75 pc, respectively.

Keywords: Open star cluster (1160); Stellar kinematics (1608)

1. INTRODUCTION

Born in giant molecular clouds (GMCs) (Lada & Lada 2003), and probably being the origins of most stars (not all stars; Ward & Kruijssen 2018; Ward et al. 2020), clusters are frequently chosen as the tracers to obtain the knowledge of the dynamical evolution of the galaxies. Investigations about the evolution and interaction about open clusters (OCs) present a deeper insight of the origin and evolution of the Galactic stars. Even for the clusters emerged from same GMC, they still may enter separated dynamical paths (Pang et al. 2020). Therefore, each OC can be a unique object to study.

One interesting feature for OCs is the long tidal tails. For young OCs ($\lesssim 100$ Myr), the relic structures of the GMCs they formed or the fast gas expulsion can be the explanations for such structures (Meingast et al. 2021; Pang et al. 2021). For relatively elder clusters ($\gtrsim 100$ Myr), two-body relaxation or external interactions, such as disk shocks, may be the main causes of the stripped members in tidal tails (Carrera et al. 2019). Dinnbier & Kroupa (2020) clas-

sified two kinds of tidal tails, tail I : formed because of gas expulsion; tail II : resulted from evaporation. A number of young OCs have been detected with tail-like structures, including IC 2391, IC 2602, NGC 2451A, NGC 2547 (Meingast et al. 2021) and NGC 2232, NGC 2451B (Pang et al. 2021) (NGC 2547 has been analyzed in both Meingast et al. 2021 and Pang et al. 2021). In addition, more and more relatively elder OCs have been revealed with tidal tails, such as Hyades (Meingast & Alves 2019; Röser et al. 2019; Jerabkova et al. 2021); NGC 6774 (Yeh et al. 2019; Pang et al. 2021); Coma Berenices (Förnkrantz et al. 2019; Tang et al. 2019); Praesepe (Röser & Schilbach 2019); NGC 2682 (Carrera et al. 2019; Gao 2020); Blanco 1 (Zhang et al. 2020; Meingast et al. 2021; Pang et al. 2021); newly discovered OC UBC 274 (Castro-Ginard et al. 2020); NGC 2506 (Gao 2020); α Per (Nikiforova et al. 2020; Meingast et al. 2021); Platais 9, Messier 39 (Meingast et al. 2021); NGC 6633 (Pang et al. 2021); NGC 2516 (Meingast et al. 2021; Pang et al. 2021); NGC 752 (Bhattacharya et al. 2021). Simulations (Chumak & Rastorguev 2006; Just et al. 2009; Küpper et al. 2010; Ernst et al. 2011; Jerabkova et al. 2021) steadily promoted our awareness of the properties of tidal tails. However, due to the low

number density comparing to the globular cluster, and the varying velocity components between cluster center and tails (Jerabkova et al. 2021), it is not easy to identify the stripped tails members for OC, especially obscured by the accuracy of parallax and absence of radial velocity.

IC 4756 is a relative old OC with age 890 ± 70 Myrs (Strassmeier et al. 2015) or $\log t = 8.987$ (Bossini et al. 2019) covered by non-homogeneous dust (Strassmeier et al. 2015). Its metallicity is close to solar value, $[\text{Fe}/\text{H}] = -0.02 \pm 0.01$ (Ting et al. 2012), $[\text{Fe}/\text{H}] = -0.01 \pm 0.10$ (Bagdonas et al. 2018). Its distance is about 478 pc (Cantat-Gaudin et al. 2018) to the Sun. Compared to the OCs with detected tidal tails : 1) IC 4756 is younger than NGC 752 (~ 1.34 Gyr; Agüeros et al. 2018) NGC 2506 (~ 2 Gyr; Rangwal et al. 2019), NGC 6774 (~ 2.5 Gyr; Curtis et al. 2013), UBC 274 (~ 3 Gyr; Castro-Ginard et al. 2020) and NGC 2682 (~ 3.6 Gyr; Bossini et al. 2019), but elder than the others; 2) farther than most of them (except NGC 2682, NGC 2506 and UBC 274. Considering the age and the low Galactic latitude $b = 5.325^\circ$ (Cantat-Gaudin et al. 2018) of this cluster, the tidal tails (tail II) are most likely to be formed already.

The aim of this paper is to detect tidal tails around IC 4756. Meanwhile, its radial density profile and the analysis of mass segregation are also studied. The structure of this paper is built as follows : Sec. 2 illustrates the constraints to extract initial data sample from *Gaia* EDR3; the methods of members selection, correction for distance, and the tails detection are described in Sec. 3; In Sec. 4, we present the photometric properties of the member candidates, the diagnosis of mass segregation and radial density profile. Finally, our main conclusions are summarized in Sec. 5.

2. DATA

With the known information of IC 4756 (Cantat-Gaudin et al. 2018), the initial sample can be restricted with the position on sky and parallax (α, δ, ϖ) accordingly. To serve our purpose of finding co-moving tidal structures, restrictions of the relative errors of proper motion (μ_α^*, μ_δ) are up to 30%. However, considering the small value of proper motion in the right ascension for IC 4756 ($\mu_\alpha^* \sim 1.26 \text{ mas} \cdot \text{yr}^{-1}$), limits on relative errors may lead to absence of stars that have small accurate μ_α^* and potentially are the member candidates. Therefore, we retain the stars which $\sigma_{\mu_\alpha^*} < 0.378 \text{ mas} \cdot \text{yr}^{-1}$. This limit is the 30% of the μ_α^* of IC 4756 and we can retain stars $\mu_\alpha^* \sim 0$. The relative errors of parallax are down to 10% to ensure the quality

of distances derived from parallax. According to the range of ϖ , the minimum error cut on ϖ is about 0.143 mas, which should not bring the same issue as in μ_α^* . In addition, the renormalized unit weight error (RUWE; Lindegren et al. 2018), provided along with *Gaia* EDR3 (Gaia Collaboration et al. 2021; Lindegren et al. 2021), are used to get the sources with fine astrometric solutions. The initial sample of about half a million stars near IC 4756 is extracted from EDR3 based on the criteria as following List 2:

- $270 < \alpha < 295, -10 < \delta < 20, 1/0.700 < \varpi < 1/0.300$;
- `parallax_over_error` > 10;
- $\sigma_{\mu_\alpha^*}/|\mu_\alpha^*| < 0.3$ or $\sigma_{\mu_\alpha^*} < 0.378$;
- $\sigma_{\mu_\delta}/|\mu_\delta| < 0.3$;
- $\text{RUWE} < 1.4$.

496,103 sources contain three *Gaia* photometric passbands, and error cuts for ($\varpi, \mu_\alpha^*, \mu_\delta$) may lead to significant incompleteness for those $G \geq 18$ mag in this sample. However, only about 6% stars with radial velocity from *Gaia* DR2. Therefore, 5D phase space with position and tangential velocity is adopted to extract co-moving stars associated with IC 4756. We use distance from Bailer-Jones et al. (2021) in the following calculation of spatial coordinates, but for those without this distance, $1/\varpi$ is adopted. Parallax zero point is calculated using the code from Lindegren et al. (2021).

3. METHODS

3.1. Member Selections

Panel (a) of Fig. 1 presents the tangential velocities distribution of the 496,103 sources around the center of IC 4756 in tangential velocity space. Dashed magenta ellipse fences out the obvious over-density, indicating the potential cluster co-moving members. It is hard to distinguish the co-moving tidal tails only with spatial coordinates due to the low number density. Therefore, we first define 5D neighbors to roughly remove a large amount of stars that do not belong to any over-density in phase space. We calculate neighbors for all 496,103 sources, which is defined in phase space $(x, y, z, \kappa \cdot \mu_\alpha^*/\varpi, \kappa \cdot \mu_\delta/\varpi)$, same as Eq. (1) in Ye et al. (2021) and the reference therein. In short, for each source, its neighbors is defined within a radius of 15 pc in (x, y, z) and a radius of 1.1 km s^{-1} in $(\kappa \cdot \mu_\alpha^*/\varpi, \kappa \cdot \mu_\delta/\varpi)$. Panel (b) of Fig. 1 shows the histogram of neighbors. The dashed magenta line represent neighbors = 3. It is clear that numerous stars

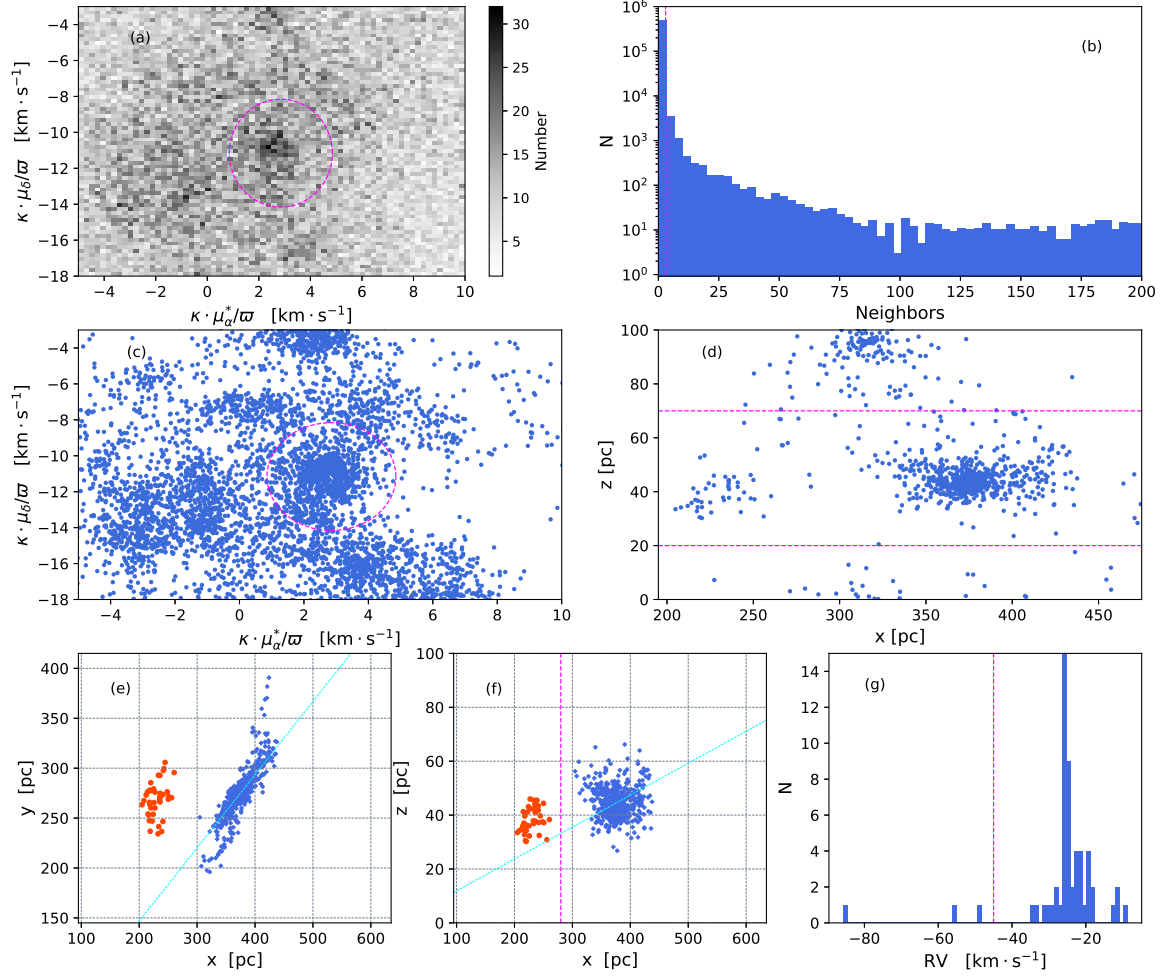


Figure 1. Steps to obtain cluster memberships for IC 4756. (a) Density map around IC 4756, a distinct overdensity is revealed inside the dashed magenta ellipse, which is centered at the predicted center calculated with parameter from Cantat-Gaudin et al. (2018). (b) The histogram plot of so called 5D neighbors for all 496,103 sources from *Gaia*. A number of individuals have neighbors ≤ 3 , indicated by dashed magenta line. (c) Tangential velocities for stars that neighbors > 3 . A bulk of stars that within the ellipse are into the next steps. (d) Overdensity in Galactic Cartesian coordinates xz plane. The center of this right-handed coordinates system is the Sun, positive x pointing to the Galactic center, positive y the Galactic rotation directions, and z to north Galactic pole. $20 \text{ pc} < z < 70 \text{ pc}$ cut leaves a more clean members. (e) Two groups clustered by HDBSCAN are shown in different colors in $x - y$ plane, IC 4756 corresponding to the blue plus signs. Line-of-sight is indicated by the cyan line. (f) Two groups from (e) in $x - z$ plane. Dashed magenta line separates them. (g) Distribution of *Gaia* DR2 radial velocities and sources on the left side of the dashed magenta line are removed.

have neighbors less than 3. Thus we can roughly remove field stars and keep 7,312 stars with neighbors > 3 into the next procedure. Taking μ_α^*, μ_δ and ϖ from Cantat-Gaudin et al. (2018) to estimate the center of tangential velocity $(\kappa \cdot \mu_\alpha^* / \varpi, \kappa \cdot \mu_\delta / \varpi)$ for IC 4756, we then extract stars within the dashed magenta ellipse in panel (c), which cover the full overdensity in tan-

gential velocity space and only contain a small fraction of contamination. The ellipse is described by the second item in List 3.1, and it is the same as in Fig. 1 panel (a). An evident overdensity is unfolded in Galactic Cartesian coordinates (centered at Sun) xz plane in panel (d), corresponding to our target cluster. Positive x in this frame points toward the Galactic center, y di-

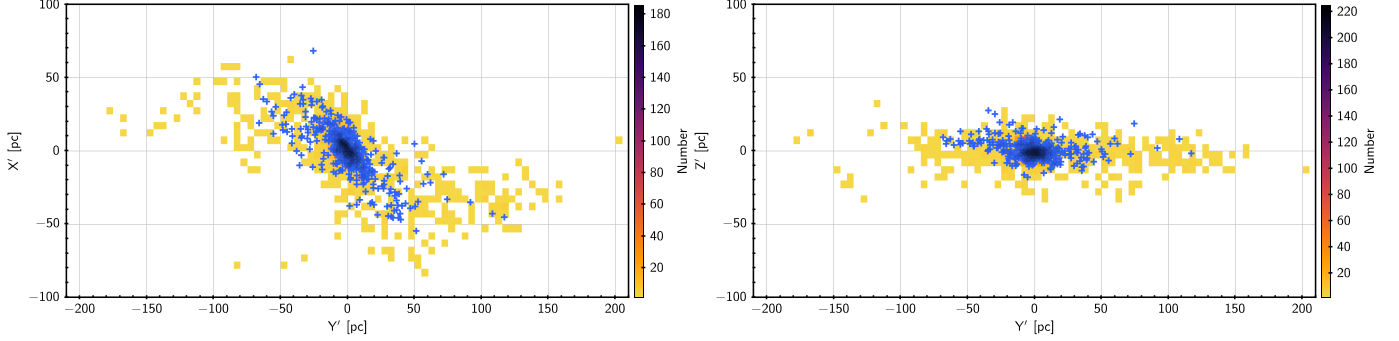


Figure 2. Member candidates for IC 4756 compared with already discovered tidal tails in (Y', X') and (Y', Z') . The color bars show the number density of tidal tails from literatures. Blue plus signs are IC 4756 memberships.

rects the local rotation, and z points to the Galactic north pole. Considering the thin distributions in z direction, we cut $20 \text{ pc} < z < 70 \text{ pc}$ (between dashed magenta lines) to avoid a number of stars that have no significant differences in tangential velocities but scattered in spatial coordinates. After the above steps, 725 stars left. Then HDBSCAN (Campello et al. 2013; McInnes et al. 2017) with `min_cluster_size = 20` is used to obtain the members of IC 4756 in (x, y, z) space. This algorithm detected two clusters : one is exactly IC 4756 (displayed with blue plus signs in panel (e-f) of Fig. 1) and the other one corresponds to the clump shown in panel (d) around $(230, 40)$ in xz plane (marked as orange dots in panel (e) and (f)). The latter is beyond the extent of IC 4756 and its tidal tails, so we do not focus on it in this paper. The cyan lines indicate the line of sight in Galactic coordinates, and the magenta line in panel (f) separates the two HDBSCAN identified clusters. The last panel shows the *Gaia* DR2 radial velocity distribution. Most stars locates around $-24.74 \text{ km}\cdot\text{s}^{-1}$ (Soubiran et al. 2018). Three sources away from the distribution center are discarded (on the left side of the dashed line). At last, we obtain 644 cluster member stars. The corresponding cuts described above are listed in List 3.1 below.

- neighbors $> 3 \rightarrow 7,312$ stars remaining;
- $\frac{(\kappa \cdot \mu_{\alpha}^* / \varpi - 2.85)^2}{2^2} + \frac{(\kappa \cdot \mu_{\delta} / \varpi + 11.16)^2}{3^2} \leq 1 \rightarrow 1,019$ stars remaining;
- $20 \text{ pc} < z < 70 \text{ pc} \rightarrow 725$ stars remaining;
- HDBSCAN;
- cut on radial velocity $\rightarrow 644$ stars remaining.

3.2. Correction for Distance

The elongated morphology of our extracted members are influenced a lot by accuracy of individual distance as indicated by the line-of-sight in panel (e) of Fig. 1. Even

we have limited the `parallax_over_error` to make a 10% relative error cut in ϖ , and adapt the distance from Bailer-Jones et al. (2021) to replace the simply inverted ϖ , the observation effect is still not completely eliminated. To moderate this impact, we follow the Bayesian approach detailed in Bailer-Jones (2015) and introduce a prior used in Carrera et al. (2019) to calculate the likelihood. This prior can be described by a sum of two parts, indicating cluster members and field stars respectively. In Eq. 1, the former exponentially decreasing term represents the field stars and the latter one indicates the cluster members.

$$P(d) \propto C \cdot d^2 e^{-\frac{d}{8[\text{kpc}]}} + (1 - C) \cdot \frac{1}{\sqrt{2\pi\sigma_d^2}} e^{-\frac{(d-d_0)^2}{2\sigma_d^2}} \quad (1)$$

d_0 is the predicted mean distance of cluster members, adopted as the inverted parallax from Cantat-Gaudin et al. (2018). σ_d is the deviation of the distances between member stars and its cluster center, as used in Pang et al. (2020, 2021). Differed from Pang et al. (2020, 2021), we set unique coefficient C for each individual. The coefficients C is the contamination fraction same as Eq. (1) in Meingast et al. (2021), like $\rho_{\text{field}} / (\rho_{\text{cluster},i} + \rho_{\text{field}})$. In a nutshell, the ρ_{field} , $\rho_{\text{cluster},i}$ are the volume number density of field stars and cluster member star i . For each cluster member, $\rho_{\text{cluster},i}$ is calculated within a radius of the distance to its seventh (7th) nearest neighbor among 644 cluster candidates. Following Meingast et al. (2021), the sample of field sources is chosen as the inner stars of the ellipse in panel (a) of Fig. 1 with the final cluster member stars removed. Because those stars are co-moving with IC 4756, but not the member candidates. ρ_{field} is derived with same definition for $\rho_{\text{cluster},i}$ but is set as the median value of this sample.

3.3. Extended Tails For IC 4756

The revised distance for each individual has then been utilized in a left-handed Galactocentric Cartesian coordinates computations. Sun is set at height $Z_{\odot} = 0.027$

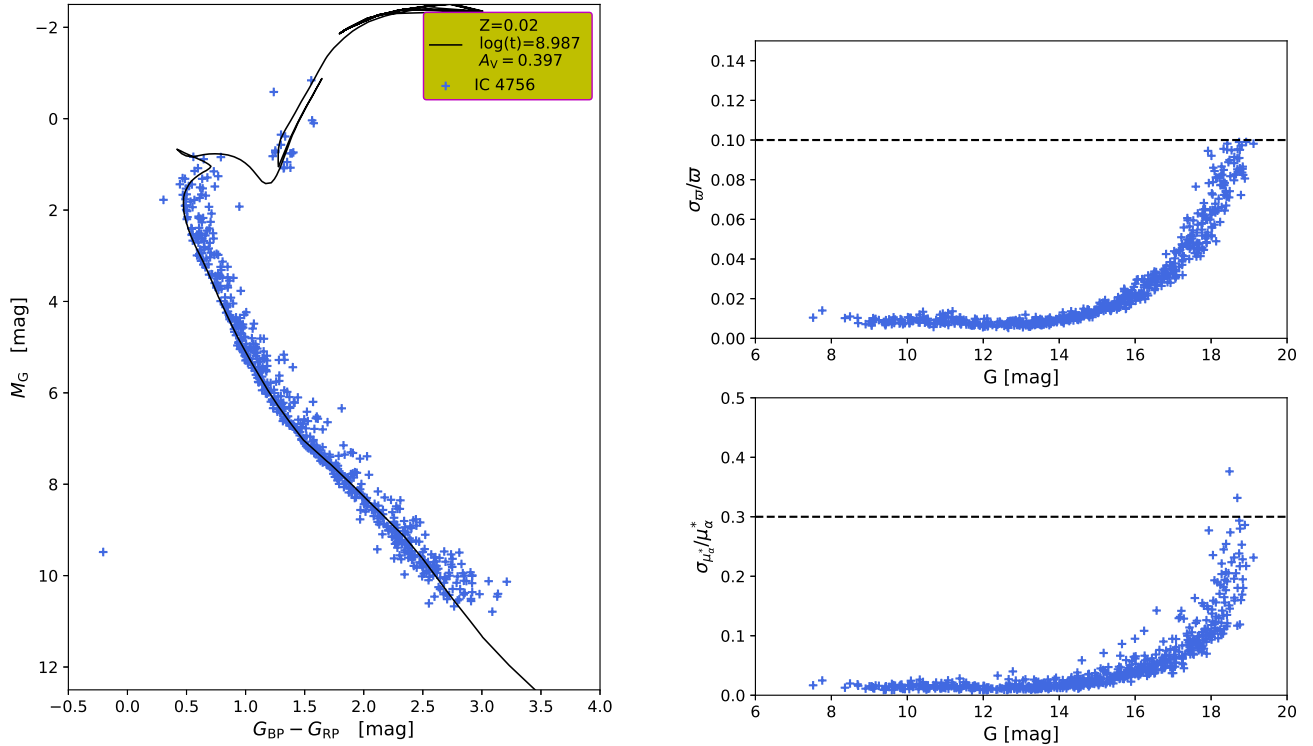


Figure 3. Left : CAMD of 644 members of IC 4756. The blue plus signs represent cluster members and PARSEC isochrone is plotted as black line. Right : Magnitude G vs. relative errors (ϖ and μ_α^*) of those members. Black dashed lines are corresponding the 30% cuts used in data extraction.

kpc (Chen et al. 2001) and at a radius of $R_\odot = 8.3$ kpc (Gillessen et al. 2009). To better compare memberships spatial distribution with the tidal tails in literatures, we rotate and translate the Galactocentric Cartesian coordinates to focus on cluster center. This new coordinates X' points from Galactic center to cluster center, Y' directs the Galactic rotation in this local, and Z' still points to the north Galactic pole. In Fig. 2, our member candidates are compared to the detected tidal tails of Hyades (Meingast & Alves 2019) and Praesepe (Röser & Schilbach 2019), which are transformed in this same coordinates as well. Member candidates of IC 4756 present quite similar distribution as the tails in Meingast & Alves (2019) and Röser & Schilbach (2019) in (X', Y', Z') space. The observation effect is effectively diminished, compared with panel (e) in Fig. 1, and two tails stand out, apparently. But the extent of tails is smaller than Meingast & Alves (2019) and Röser & Schilbach (2019), only up to 180 pc for total length. In addition, the leading tail is slightly longer than the trailing tail. All the member candidates demonstrate a S-shape in (X', Y') . As shown in Fig. 2,

most stars are gathered around dozens of parsecs and a relatively much lower number density in the tails.

4. RESULTS

4.1. Color-Absolute-Magnitude Diagram

All 644 member candidates are drawn in color-absolute magnitude diagram (CAMD) as $G_{BP} - G_{RP}$ and $M_G = G - 5 \lg(d/10)$, where d is the corrected distance in pc. PARSEC (version 1.2S) isochrone¹ (Bressan et al. 2012; Chen et al. 2014, 2019) with $Z = 0.02$, $\log t = 8.987$, $A_V = 0.397$ (Bossini et al. 2019) is together shown in left panel of Fig. 3. A clean CAMD is fitted excellently with the PARSEC isochrone for main sequence and giants branch. Noted that we do not apply any extinction for these *Gaia* EDR3 passbands, and $A_V = 0.397$ is used in PARSEC isochrone, so the sequence of cluster members may be less scattered when accurate extinction parameters are adopted. Another proof for the correctly clean member selection

¹ <http://stev.oapd.inaf.it/cgi-bin/cmd>

is a two-dimensional KS test (Peacock 1983). It can inspect member candidates to verify that the members are not casually selected from the initial sample in Sec. 2. Following Meingast & Alves (2019), we get a mean p -value about 10^{-18} between our candidates and the randomly collections (all have same length as our candidates selection) taken from initial sample. The mean value is obtained from 10,000 tests. The mean value between two random sets is typically about 0.52. The right panel of Fig. 3 shows that our member candidates may suffer incompleteness for fainter stars $G \approx 18$ mag ($M_G \approx 9.7$ mag), according to the relative errors cuts in Sec. 2.

4.2. Mass Segregation

Stars with different mass may be segregated in a cluster, where the more massive stars assembled in the core of the cluster and less massive individuals tends to evaporated from it (Hillenbrand & Hartmann 1998). It might be from the primordial segregation (Pavlík et al. 2019) when they were formed, or dynamical consequence (Allison et al. 2009). Allison et al. 2009 presented the approach without previous knowledge about the center position of the cluster to do a quantitative analysis for mass segregation. The mass segregation is detected by analyze the mean mass of each individual in different annuli. A rough estimate for stellar mass for each member of IC 4756 is derived through the CAMD and PARSEC isochrone. For each individual, its mass is adopted as the mean mass of two nearest stars from isochrone. The top panel of Fig. 4 presents the mean stellar mass as a function of distance from the cluster center. The distance of each annulus from the center is calculated with three-dimensional coordinates (X' , Y' , Z') centered at (0, 0, 0). From Fig. 4 top panel, we can see a slight tendency that the mean mass declines about dozens of pc away from the center. But due to the large dispersions shown as error bars in the figure, it is not convincing to conclude a mass segregation here. Besides, this tendency disappears out 50 pc, grey shadow. It might be the reason that few members are beyond 50 pc (93% stars are within 50 pc). The bottom panel of Fig. 4 presents the three mass functions of the members for different distance from the center. The members are divided into three groups according to the distance from center r : $r < 10$ pc, $10 \leq r < 50$ pc, and $r \geq 50$ pc, which are presented as blue, magenta, and green lines, respectively. The y axis is the fraction of numbers in each bin. Although it displays no inclination for the group of $r \geq 50$ pc, this figure certainly reveals the upward and downward trends of $r < 10$ pc and $10 \leq r < 50$ pc MFs for more massive stars. They agree with the tendency

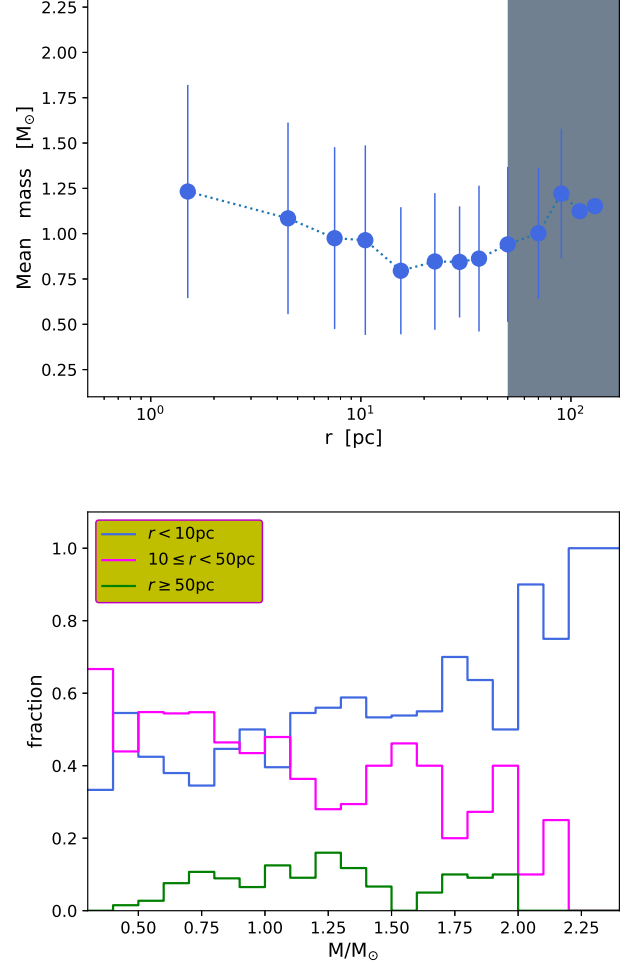


Figure 4. Top panel : Mean stellar mass of IC 4756 vs. distance from the cluster center r in different annuli. The intervals are larger when stars are far away from the center. The standard deviation is presented as the error bar in each annulus. The grey shadow represents the area that $r \geq 50$ pc. Bottom panel : mass functions for $r < 10$ pc, $10 \leq r < 50$ pc, and $r \geq 50$ pc, shown as blue, magenta and green lines, respectively. Y-axis is the fraction of numbers in each bin.

shown in the top panel of Fig. 4. Therefore, we conclude the mass segregation in IC 4756.

4.3. Radial Density Profile

Kharchenko et al. (2013) derived the core radii and the tidal radii of OCs according to a King density model (King 1962). However, considering the long extended structure in IC 4756, it is not appropriate to construct its radial density profile using the power law from King (1962). In most cases, not all of them, the parameter of density law, tidal radius, is close to the Jacobi radius (distance between a star cluster center and the Lagrange points), which indicates the boundary of gravitationally

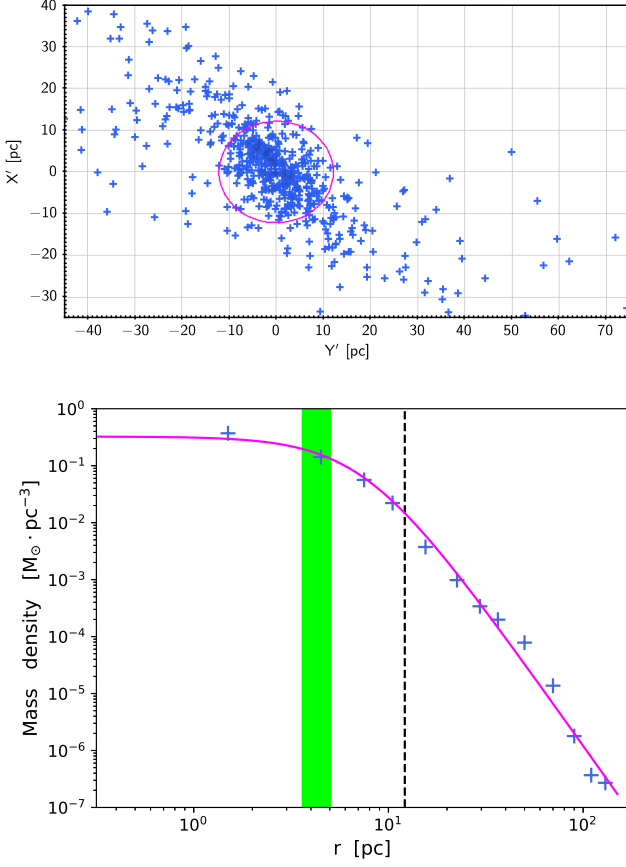


Figure 5. Top panel : The distribution of member stars of IC 4756 in $X'Y'$ space. Tidal radius is presented as the magenta circle. Bottom panel : Radial mass density of IC 4756 vs. distance from the cluster center in different annuli. The intervals of distance are same as those in Fig. 4. The magenta curve is the fitted model (Elson et al. 1987) with a core radius of 4.33 ± 0.75 pc, shown as the green shadow. Tidal radius r_t is also presented as vertical black dashed line.

bound and unbound stars in a star cluster. For our cluster members, we use Eq. 2 (Pinfield et al. 1998) to estimate the value of this gravitationally bound radius, which is adopted as tidal radius in this paper.

$$r_t = \left[\frac{GM_{\text{total}}}{2(A-B)^2} \right]^{1/3}. \quad (2)$$

The M_{total} in Eq. 2 is the total mass of cluster members. Gravitational constant $G = 4.3 \times 10^{-6}$ kpc $(\text{km s}^{-1})^2 M_{\odot}^{-1}$, and the Oort constants $A = 15.3 \pm 0.4$ kpc $^{-1}$ km s $^{-1}$, $B = -11.9 \pm 0.4$ kpc $^{-1}$ km s $^{-1}$ are from Bovy 2017. In this way, we obtain the tidal radius $r_t = 12.13$ pc, shown as the magenta circle in top panel of Fig. 5. We present the members closer to the center part in $X'Y'$, comparing to the left panel of Fig. 2, in order to give a clearer view around the circle of tidal radius.

Stars inside the circle are distributed more compactly. 56% members concentrate inside r_t , which contribute 60% mass of IC 4756. As considerable parts of members and mass of IC 4756 are beyond the tidal radius and IC 4756 is about 1 Gyr old, we presume that IC 4756 is undergoing disruption.

The radial density profile is also computed. It decreases drastically as the distance to cluster center increases, but with the long tidal tails, it is more appropriate to be compared with the power law from Elson, Fall, Freeman model Elson et al. (1987), hereafter EFF model. We take radial mass density instead of the surface brightness in EFF model, and the power law is presented in Eq. 3,

$$\rho(r) = \rho_0 \cdot \left(1 + (r/a)^2\right)^{-\gamma/2}, \quad (3)$$

where ρ_0 is the mass density of a cluster in its center, a is related to the core radius and γ is the index of slope. The core radius r_c indicates the sphere where the surface brightness of a cluster falls by half of its central surface brightness. In our situation, we adopt the relation $\rho(r_c) = 1/2\rho_0$ to obtain the core radius as Eq. 4,

$$r_c = a \cdot \left(2^{2/\gamma} - 1\right)^{1/2}, \quad (4)$$

same as Eq. 22 in Elson et al. (1987). Radial density profile of IC 4756 and the analytical model with fitted parameters are presented in bottom panel of Fig. 5. The derived density $\rho_0 = 0.325 \pm 0.130 M_{\odot} \cdot \text{pc}^{-3}$ is consistent with the central density from 644 members ($0.364 M_{\odot} \cdot \text{pc}^{-3}$), which is the density within 2 pc from the center. The core radius $r_c = 4.33 \pm 0.75$ pc. The green belt represents r_c and its error. The curve matches up perfectly with the real density profile.

5. SUMMARY

We discover the extended tidal tails of IC 4756 using the astrometry from *Gaia* EDR3. The method to determine the co-moving member candidates of IC 4756 contains defined neighbors in $(x, y, z, \kappa \cdot \mu_{\alpha}^*/\varpi, \kappa \cdot \mu_{\delta}/\varpi)$ and HDBSCAN, and other cuts in various parameter spaces. 644 member stars are identified as members of IC 4756. After distance corrections using a Bayesian approach, evident two tidal tails extend up to 180 pc in total length and present a clear S-shape in (X', Y') space. Hundreds of stars are found beyond the tidal radius, $r_t \sim 12.13$ pc. The shape and position of tidal tails are coincides with literatures. A clean sequence in CAMD and 2-D KS test further prove the validity of our selections of cluster members and the right age

$\log t = 8.987$ in literatures. Using mean mass in different annuli and the mass functions, we detect the evidence of mass segregation in this cluster. The radial mass density profile fits perfectly with EFF model, obtaining a core radius $r_c = 4.33 \pm 0.75$ pc.

ACKNOWLEDGMENTS

Xianhao Ye thanks Zhenyu Wu and Xiaoying Pang for helpful discussions. This study is supported by CMS-CSST-2021-B05, National Key R&D Program of China No. 2019YFA0405502 and the National Natural Science Foundation of China under grant No. 11988101, 11973048, 11927804, 11890694. This work has made use of data from the European Space Agency (ESA) mission *Gaia* (<https://www.cosmos.esa.int/gaia>), processed by the *Gaia* Data Processing and Analysis Consortium (DPAC, <https://www.cosmos.esa.int/web/gaia/dpac/consortium>). The *Gaia* archive website is <https://archives.esac.esa.int/gaia>. We also acknowledge the support from the 2m Chinese Space Station Telescope project.

Software: Astropy (Astropy Collaboration et al. 2013), Galpy (Bovy 2015), HDBSCAN (Campello et al. 2013; McInnes et al. 2017), Matplotlib (Hunter 2007), Numpy (van der Walt et al. 2011), Pandas (McKinney 2010), Scipy (Virtanen et al. 2020), Scikit-learn (Pedregosa et al. 2012), Topcat (Taylor 2005)

REFERENCES

- Agüeros, M. A., Bowsher, E. C., Bochanski, J. J., et al. 2018, *ApJ*, 862, 33. doi: [10.3847/1538-4357/aac6ed](https://doi.org/10.3847/1538-4357/aac6ed)
- Allison, R. J., Goodwin, S. P., Parker, R. J., et al. 2009, *ApJL*, 700, L99. doi: [10.1088/0004-637X/700/2/L99](https://doi.org/10.1088/0004-637X/700/2/L99)
- Allison, R. J., Goodwin, S. P., Parker, R. J., et al. 2009, *MNRAS*, 395, 1449. doi: [10.1111/j.1365-2966.2009.14508.x](https://doi.org/10.1111/j.1365-2966.2009.14508.x)
- Astropy Collaboration, Robitaille, T. P., Tollerud, E. J., et al. 2013, *A&A*, 558, A33. doi: [10.1051/0004-6361/201322068](https://doi.org/10.1051/0004-6361/201322068)
- Bagdonas, V., Drazdauskas, A., Tautvaišienė, G., et al. 2018, *A&A*, 615, A165. doi: [10.1051/0004-6361/201832695](https://doi.org/10.1051/0004-6361/201832695)
- Bailer-Jones, C. A. L. 2015, *PASP*, 127, 994. doi: [10.1086/683116](https://doi.org/10.1086/683116)
- Bailer-Jones, C. A. L., Rybizki, J., Fouesneau, M., et al. 2021, *AJ*, 161, 147. doi: [10.3847/1538-3881/abd806](https://doi.org/10.3847/1538-3881/abd806)
- Bhattacharya, S., Agarwal, M., Rao, K. K., et al. 2021, *MNRAS*, 505, 1607. doi: [10.1093/mnras/stab1404](https://doi.org/10.1093/mnras/stab1404)
- Bossini, D., Vallenari, A., Bragaglia, A., et al. 2019, *A&A*, 623, A108. doi: [10.1051/0004-6361/201834693](https://doi.org/10.1051/0004-6361/201834693)
- Bovy, J. 2015, *ApJS*, 216, 29. doi: [10.1088/0067-0049/216/2/29](https://doi.org/10.1088/0067-0049/216/2/29)
- Bovy, J. 2017, *MNRAS*, 468, L63. doi: [10.1093/mnras/rlx027](https://doi.org/10.1093/mnras/rlx027)
- Bressan, A., Marigo, P., Girardi, L., et al. 2012, *MNRAS*, 427, 127. doi: [10.1111/j.1365-2966.2012.21948.x](https://doi.org/10.1111/j.1365-2966.2012.21948.x)
- Campello, R. J. G. B., Moulavi, D., & Sander, J. 2013, in *Advances in Knowledge Discovery and Data Mining*, eds. J. Pei, V. S. Tseng, L. Cao, H. Motoda, & G. Xu (Berlin, Heidelberg: Springer, Berlin Heidelberg), 160

- Cantat-Gaudin, T., Jordi, C., Vallenari, A., et al. 2018, A&A, 618, A93. doi: [10.1051/0004-6361/201833476](https://doi.org/10.1051/0004-6361/201833476)
- Castro-Ginard, A., Jordi, C., Luri, X., et al. 2020, A&A, 635, A45. doi: [10.1051/0004-6361/201937386](https://doi.org/10.1051/0004-6361/201937386)
- Carrera, R., Pasquato, M., Vallenari, A., et al. 2019, A&A, 627, A119. doi: [10.1051/0004-6361/201935599](https://doi.org/10.1051/0004-6361/201935599)
- Chen, B., Stoughton, C., Smith, J. A., et al. 2001, ApJ, 553, 184. doi: [10.1086/320647](https://doi.org/10.1086/320647)
- Chen, Y., Girardi, L., Bressan, A., et al. 2014, MNRAS, 444, 2525. doi: [10.1093/mnras/stu1605](https://doi.org/10.1093/mnras/stu1605)
- Chen, Y., Girardi, L., Fu, X., et al. 2019, A&A, 632, A105. doi: [10.1051/0004-6361/201936612](https://doi.org/10.1051/0004-6361/201936612)
- Chumak, Y. O. & Rastorguev, A. S. 2006, Astronomy Letters, 32, 446. doi: [10.1134/S1063773706070036](https://doi.org/10.1134/S1063773706070036)
- Curtis, J. L., Wolfgang, A., Wright, J. T., et al. 2013, AJ, 145, 134. doi: [10.1088/0004-6256/145/5/134](https://doi.org/10.1088/0004-6256/145/5/134)
- Dinnbier, F. & Kroupa, P. 2020, A&A, 640, A84. doi: [10.1051/0004-6361/201936570](https://doi.org/10.1051/0004-6361/201936570)
- Elson, R. A. W., Fall, S. M., & Freeman, K. C. 1987, ApJ, 323, 54. doi: [10.1086/165807](https://doi.org/10.1086/165807)
- Ernst, A., Just, A., Berczik, P., et al. 2011, A&A, 536, A64. doi: [10.1051/0004-6361/201118021](https://doi.org/10.1051/0004-6361/201118021)
- Fürnkranz, V., Meingast, S., & Alves, J. 2019, A&A, 624, L11. doi: [10.1051/0004-6361/201935293](https://doi.org/10.1051/0004-6361/201935293)
- Gaia Collaboration, Brown, A. G. A., Vallenari, A., et al. 2021, A&A, 649, A1. doi: [10.1051/0004-6361/202039657](https://doi.org/10.1051/0004-6361/202039657)
- Gao, X. 2020, PASJ, 72, 47. doi: [10.1093/pasj/psaa031](https://doi.org/10.1093/pasj/psaa031)
- Gao, X. 2020, ApJ, 894, 48. doi: [10.3847/1538-4357/ab8560](https://doi.org/10.3847/1538-4357/ab8560)
- Gillessen, S., Eisenhauer, F., Trippe, S., et al. 2009, ApJ, 692, 1075. doi: [10.1088/0004-637X/692/2/1075](https://doi.org/10.1088/0004-637X/692/2/1075)
- Hillenbrand, L. A. & Hartmann, L. W. 1998, ApJ, 492, 540. doi: [10.1086/305076](https://doi.org/10.1086/305076)
- Hunter, J. D. 2007, Computing in Science and Engineering, 9, 90. doi: [10.1109/MCSE.2007.55](https://doi.org/10.1109/MCSE.2007.55)
- Jerabkova, T., Boffin, H. M. J., Beccari, G., et al. 2021, A&A, 647, A137. doi: [10.1051/0004-6361/202039949](https://doi.org/10.1051/0004-6361/202039949)
- Just, A., Berczik, P., Petrov, M. I., et al. 2009, MNRAS, 392, 969. doi: [10.1111/j.1365-2966.2008.14099.x](https://doi.org/10.1111/j.1365-2966.2008.14099.x)
- Kharchenko, N. V., Piskunov, A. E., Schilbach, E., et al. 2013, A&A, 558, A53. doi: [10.1051/0004-6361/201322302](https://doi.org/10.1051/0004-6361/201322302)
- King, I. 1962, AJ, 67, 471. doi: [10.1086/108756](https://doi.org/10.1086/108756)
- Küpper, A. H. W., Kroupa, P., Baumgardt, H., et al. 2010, MNRAS, 401, 105. doi: [10.1111/j.1365-2966.2009.15690.x](https://doi.org/10.1111/j.1365-2966.2009.15690.x)
- Lada, C. J. & Lada, E. A. 2003, ARA&A, 41, 57. doi: [10.1146/annurev.astro.41.011802.094844](https://doi.org/10.1146/annurev.astro.41.011802.094844)
- Lindgren, L. 2018, technical note GAIA-C3-TN-LU-LL-124
- Lindgren, L., Klioner, S. A., Hernández, J., et al. 2021, A&A, 649, A2. doi: [10.1051/0004-6361/202039709](https://doi.org/10.1051/0004-6361/202039709)
- Lindgren, L., Bastian, U., Biermann, M., et al. 2021, A&A, 649, A4. doi: [10.1051/0004-6361/202039653](https://doi.org/10.1051/0004-6361/202039653)
- McInnes, L., Healy, J., & Astels, S. 2017, JOSS, 2, 205. doi: [10.21105/joss.00205](https://doi.org/10.21105/joss.00205)
- McKinney, W. 2010, in Proc. of the 9th Python in Science Conf. (SciPy 2010), ed. S. van der Walt & J. Millman, 56, doi: [10.25080/Majora-92bf1922-00a](https://doi.org/10.25080/Majora-92bf1922-00a)
- Meingast, S. & Alves, J. 2019, A&A, 621, L3. doi: [10.1051/0004-6361/201834622](https://doi.org/10.1051/0004-6361/201834622)
- Meingast, S., Alves, J., & Rottensteiner, A. 2021, A&A, 645, A84. doi: [10.1051/0004-6361/202038610](https://doi.org/10.1051/0004-6361/202038610)
- Nikiforova, V. V., Kulesh, M. V., Seleznev, A. F., et al. 2020, AJ, 160, 142. doi: [10.3847/1538-3881/aba753](https://doi.org/10.3847/1538-3881/aba753)
- Pang, X., Li, Y., Tang, S.-Y., et al. 2020, ApJL, 900, L4. doi: [10.3847/2041-8213/abad28](https://doi.org/10.3847/2041-8213/abad28)
- Pang, X., Li, Y., Yu, Z., et al. 2021, ApJ, 912, 162. doi: [10.3847/1538-4357/abeaac](https://doi.org/10.3847/1538-4357/abeaac)
- Pavlík, V., Kroupa, P., & Šubr, L. 2019, A&A, 626, A79. doi: [10.1051/0004-6361/201834265](https://doi.org/10.1051/0004-6361/201834265)
- Peacock, J. A. 1983, MNRAS, 202, 615. doi: [10.1093/mnras/202.3.615](https://doi.org/10.1093/mnras/202.3.615)
- Pedregosa, F., Varoquaux, G., Gramfort, A., et al. 2012, <https://arxiv.org/abs/1201.0490>
- Pinfield, D. J., Jameson, R. F., & Hodgkin, S. T. 1998, MNRAS, 299, 955. doi: [10.1046/j.1365-8711.1998.01754.x](https://doi.org/10.1046/j.1365-8711.1998.01754.x)
- Rangwal, G., Yadav, R. K. S., Durgapal, A., et al. 2019, MNRAS, 490, 1383. doi: [10.1093/mnras/stz2642](https://doi.org/10.1093/mnras/stz2642)
- Röser, S., Schilbach, E., & Goldman, B. 2019, A&A, 621, L2. doi: [10.1051/0004-6361/201834608](https://doi.org/10.1051/0004-6361/201834608)
- Röser, S. & Schilbach, E. 2019, A&A, 627, A4. doi: [10.1051/0004-6361/201935502](https://doi.org/10.1051/0004-6361/201935502)
- Soubiran, C., Cantat-Gaudin, T., Romero-Gómez, M., et al. 2018, A&A, 619, A155. doi: [10.1051/0004-6361/201834020](https://doi.org/10.1051/0004-6361/201834020)
- Strassmeier, K. G., Weingrill, J., Granzer, T., et al. 2015, A&A, 580, A66. doi: [10.1051/0004-6361/201525756](https://doi.org/10.1051/0004-6361/201525756)
- Tang, S.-Y., Pang, X., Yuan, Z., et al. 2019, ApJ, 877, 12. doi: [10.3847/1538-4357/ab13b0](https://doi.org/10.3847/1538-4357/ab13b0)
- Taylor, M. B. 2005, adass XIV, 347, 29
- Ting, Y.-S., De Silva, G. M., Freeman, K. C., et al. 2012, MNRAS, 427, 882. doi: [10.1111/j.1365-2966.2012.22028.x](https://doi.org/10.1111/j.1365-2966.2012.22028.x)
- van der Walt, S., Colbert, S. C., & Varoquaux, G. 2011, Computing in Science and Engineering, 13, 22. doi: [10.1109/MCSE.2011.37](https://doi.org/10.1109/MCSE.2011.37)
- Virtanen, P., Gommers, R., Oliphant, T. E., et al. 2020, Nature Methods, 17, 261. doi: [10.1038/s41592-019-0686-2](https://doi.org/10.1038/s41592-019-0686-2)
- Ward, J. L. & Kruijssen, J. M. D. 2018, MNRAS, 475, 5659. doi: [10.1093/mnras/sty117](https://doi.org/10.1093/mnras/sty117)
- Ward, J. L., Kruijssen, J. M. D., & Rix, H.-W. 2020, MNRAS, 495, 663. doi: [10.1093/mnras/staa1056](https://doi.org/10.1093/mnras/staa1056)
- Ye, X., Zhao, J., Liu, J., et al. 2021, AJ, 161, 8. doi: [10.3847/1538-3881/abc61a](https://doi.org/10.3847/1538-3881/abc61a)

Yeh, F. C., Carraro, G., Montalto, M., et al. 2019, AJ, 157,
115. doi: [10.3847/1538-3881/aaff6c](https://doi.org/10.3847/1538-3881/aaff6c)

Zhang, Y., Tang, S.-Y., Chen, W. P., et al. 2020, ApJ, 889,
99. doi: [10.3847/1538-4357/ab63d4](https://doi.org/10.3847/1538-4357/ab63d4)